Verification of the Part-Composite Approach for Modeling the Multi-Layered Structure of a Rolling Truck Tire

Shahram Shokouhfar[1], Subhash Rakheja[1], Moustafa El-Gindy[2]

[1] Department of Mechanical and Industrial Engineering, Concordia University, Montreal, Canada
[2] Department of Automotive, Mechanical and Manufacturing Engineering, UOIT, Oshawa, Canada

Abstract

Accurate modeling of a truck tire for predicting dynamic characteristics requires an adequate representation of its composite plies. This study compares two approaches in modeling the multi-layered structure of a rolling radial-ply truck tire using LS-DYNA. In the first approach, different layers in the tire structure are modeled using individual elements; whereas, in the second, all layers are represented by a single element with layered configuration managed by the PART_COMPOSITE keyword. Hence, in this article, these tire models are named as the Individual-Element (IE) model versus the Part-Composite (PC) model. In the Individual-Element (IE) model, the carcass and belt plies are formulated using layers of isotropic solids representing rubber matrix, together with separate layers of orthotropic shells describing fiber-reinforced composite plies. In the Part-Composite (PC) model, however, the carcass and belt plies are simplified to a single layer made of shell elements with layered configuration using the PART_COMPOSITE keyword. This keyword allows to define stacks of plies with pertinent material properties, thicknesses and fiber orientations to manage the integration rule through the thickness of a composite part. The Part-Composite (PC) model was then verified to be in reasonable agreement with the Individual-Element (IE) model in predicting the load-deflection, cornering force/moment and modal characteristics of a truck tire. The validities of the tire models are also evaluated by comparing their simulation results with the reported experimental data. The Individual-Element (IE) model has the potential to be applied as a reliable virtual tool to study the influences of various operating and design parameters upon the tire dynamic characteristics. However, the large number of elements in such a detailed model makes it computationally expensive. With the Part-Composite (PC) model, the computational efficiency was remarkably improved since replacing several individual elements with one layered element reduced the total number of elements and thus the computational demand.

Keywords: Rolling truck tire model; multi-layered composite tire structure; dynamic tire properties; finite element; LS-DYNA; PART_COMPOSITE

1 Introduction

Dynamic performance characteristics of ground-vehicles strongly rely on the forces/moments arising from the interactions of the pneumatic tires with the road. These forces/moments depend on the tire complex structure and material properties as well as a number of operating parameters such as the tire inflation pressure, vertical load, rolling speed and road friction. Widely different methods of modeling pneumatic tires with varying complexities have been proposed to predict the tire forces/moments for applications in vehicle design and dynamic analyses.

The reported tire models can be classified into physical, phenomenological and structural models. The physical tire models employed mass-spring-damper elements to describe the tire forces as functions of tire deformations, road profile, travel speed, road friction, tire pressure and vertical load. Early physical models estimated the tire vertical behavior for applications in vehicle ride simulations [1–4]. Some more advanced models could describe the in-plane [5] and out-of-plane [6] dynamics of the tire to predict the longitudinal and lateral forces in order to be used in traction/braking and cornering simulations. Phenomenological models, however, used regression-based formulations to describe the tire forces/moments under a defined set of operating conditions. Among the reported phenomenological models, the Magic Formula [7] is most widely used for analyses of vehicle braking and steering responses under widely varying operating conditions. The physical and phenomenological models can yield effective predictions of the tire forces/moments and are thus well-suited for vehicle dynamics analyses, while their reliabilities highly depend on a number of model parameters which must be accurately identified and calibrated using the measured tire properties [8, 9].

The physical and phenomenological tire models could only provide estimations of global tire properties. However, these models could not yield navigations towards design of pneumatic tires as they did not directly consider the geometric, structural and material properties of tires. Consequently, a vast number of structural models have been proposed for the purpose of tire design and developments. These models have used the Finite Element (FE) methods, which allow modeling of the tire structure, geometry and material properties. The tire complex structure has been described using widely different methods. In some studies, the tire was modeled as a simple inflated airbag using a single layer of membrane elements with orthotropic material. These models could approximate the global performance of the tire in durability [10], cornering [11] and crash simulations [12] with a reasonable computational cost. A number of structural tire models have taken into account the multi-layered composite structure of the carcass and belt plies [13–17]. In some of these models, the carcass and belt plies are represented using the discrete reinforcement technique [15], where the rubber matrix is described by isotropic solid elements and the fiber-reinforced layers by orthotropic shell elements with equivalent material properties determined from those of the rubber compound and twisted cords [13, 15, 18, 19]. This technique permitted the analyses of stresses/strains in the rubber matrix and the fiber-reinforced layers [15]. In some more detailed models, the reinforcing fibers in the carcass and belt plies were directly modeled using beam elements, being connected to the isotropic elastic shell elements representing the rubber matrix via shared nodes [20]. This method permitted to define separate material properties for the fibers and the containing rubber matrix. These detailed models could yield accurate predictions of the tire dynamic characteristics when being employed in a tire testing simulation. However, considering such a high level of complexity remarkably increased the total number of elements resulting in expensive computational cost.

The primary motivation for this study comes from the desire for a simplified but still reliable tire model to be used in a virtual tire testing system with reasonable computational demand. Such a simplified and efficient tire model can be employed in durability and vehicle crash simulations as well as in analyzing the interactions of a rolling tire with deformable terrains such as soft soils, where using a detailed tire model may seem impractical due to expensive computational costs.

In this study, two different tire models are developed for predicting the tire vertical, cornering and modal properties. In the first model, different layers of the carcass and belt are modeled using individual elements, with solid elements for the rubber matrix and shell elements for the reinforcements. In the second model, however, all the layers in the carcass and belt are simplified to a single shell element having layered configuration, which is managed by the PART_COMPOSITE keyword. For the two modeling approaches to be comparable, all the material types and properties used for different layers of the carcass and belt as well as those applied to the bead fillers and the tread are defined for both the tire models in an identical manner. The simulation results predicted by the two models are finally evaluated through comparing with each other as well as with the reported experimental data in terms of load-deflection, cornering force/moment and modal characteristics.

2 Finite Element Modeling

2.1 Tire Strucutre

The tire selected for the finite element analyses in this study is a 295/75R22.5 radial-ply truck tire. Two modeling approaches are implemented using LS-DYNA to represent the multi-layered structure of the chosen tire in order to predict its vertical, cornering and modal properties. The models are formulated considering the tire geometry and its complex structure including the bead fillers, tread, carcass and belt. Fig. 1 compares the cross-sections considered for the two models. In both models, the bead fillers and the tread are represented using solid elements with rubber material behavior. The difference between the models is in formulating the carcass and belt composite plies. In the first model, different layers in carcass and belt are described using individual elements; whereas, in the second model, all layers are represented by a single element with layered configuration managed by the PART_COMPOSITE keyword. Hence, throughout this article, these models are called the Individual-Element (IE) model and the Part-Composite (PC) model, respectively.

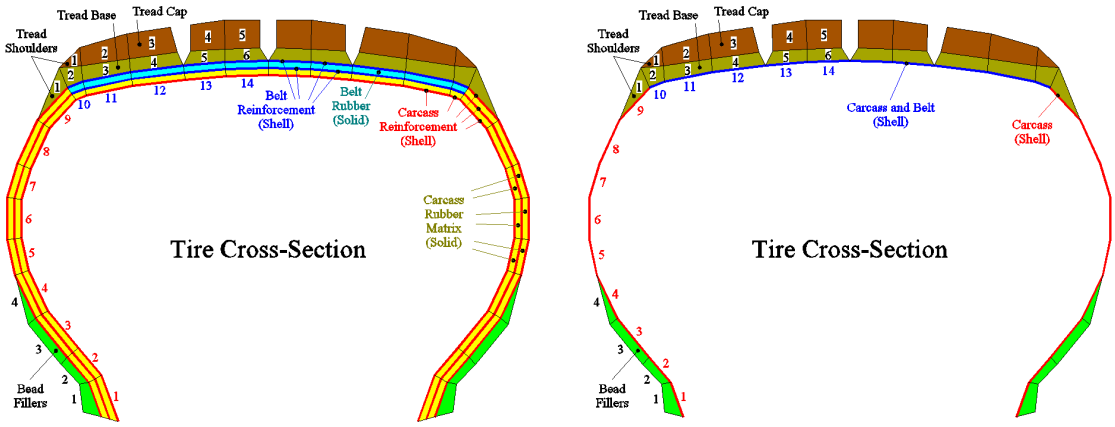

(a) Individual-Element (IE) model (b) Part-Composite (PC) model

Fig. 1: Cross-sections of the tire models

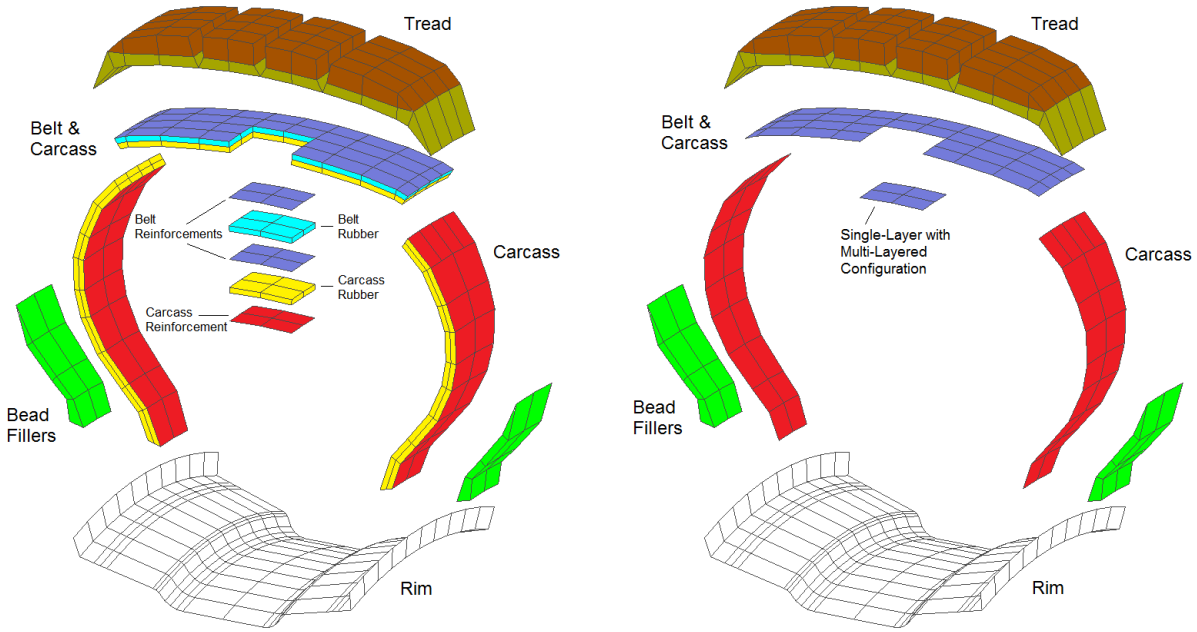

(a) Individual-Element (IE) model structure (b) Part-Composite (PC) model structure

Fig. 2: Multi-layered composite structures of the tire models

2.1.1 Individual-Element (IE) Model

Fig. 1(a) illustrates the cross-section considered for the Individual-Element (IE) model. The two layers of solid elements (regions 1 to 9) represent the carcass rubber matrix in the sidewalls, being reinforced by three layers of composite shell elements with radial cords. Two layers of solid elements (regions 10 to 14) represent the belt layers, where the upper layer accounts for the belt rubber matrix sandwiched between two layers of composite shell elements reinforced by cords with $\pm 22^{\circ}$ angles. The lower solid layer represents the carcass rubber matrix below the belt, which is also reinforced by a layer of composite shell elements with radial cords. In this model, the carcass and belt plies are formulated using the Discrete Reinforcement technique [15], where the rubber matrix is represented by solid elements and the reinforcements are discretely modeled using composite shell elements, as shown in Fig. 2(a). This approach allows for stress/strain analyses for the individual matrix and the reinforcements. The matrix and the reinforcements

are considered to be fully bonded by defining the shared nodes at the interface of the two layers. This assumption is considered valid since the study was not concerned with delamination of the plies, which rarely occurs in normal operating conditions.

2.1.2 Part-Composite (PC) Model

As shown in Fig. 2(b), in the Part-Composite (PC) model, the carcass and belt plies are simplified to a single part made of shell elements with layered configuration using the PART_COMPOSITE keyword. This keyword allows to define stacks of plies in a single shell element and is able to manage the element formulation and the integration rule through the thickness of the layered element. Table 1 summarizes the material types, thicknesses and fiber orientations for different layers of carcass and belt in the Part-Composite (PC) model, which are defined identical to those of the Individual-Elements (IE) model.

Table 1: Multi-layered configuration considered in the Part-Composite (PC) model

Regions 1 to 9 in Fig. 1 (b)				Regions 10 to 14 in Fig. 1(b)			
Layer	Material	Thickness	Angle	Layer	Material	Thickness	Angle
Carcass Reinforcement	Orthotropic	0.33 mm	90°	Belt Reinforcement	Orthotropic	1.50 mm	$+22^\circ$
Carcass Rubber	Isotropic	4.00 mm	—	Belt Rubber	Isotropic	4.00 mm	—
Carcass Reinforcement	Orthotropic	0.33 mm	90°	Belt Reinforcement	Orthotropic	1.50 mm	-22°
Carcass Rubber	Isotropic	4.00 mm	—	Carcass Rubber	Isotropic	4.00 mm	—
Carcass Reinforcement	Orthotropic	0.33 mm	90°	Carcass Reinforcement	Orthotropic	1.00 mm	90°

For each tire model, the 3D mesh is made of equal sectors via spinning the cross-section mesh about the tire axis in equal increments. By reducing the spinning increment, a refined mesh is used for the outer circumferential regions contacting the road, as shown in Fig. 3. Creating a mesh with 96 sectors and refining to 192 divisions for the outer circumferential regions (1 to 9 in Fig. 1), the total number of elements for the Individual-Element (IE) model becomes 24192, which is 2.74 times greater than that of the corresponding Part-Composite (PC) model having 8832 elements.

As shown in Fig. 3(a), due to applying different number of circumferential divisions for the coarse and refined portions of the mesh, small gaps are formed resulting in a number of free edges for the elements involving the gaps. The initial positions of the nodes belonging to the free edges of the refined elements are modified in order to obviate the gaps, as illustrated in Fig. 3(b). Moreover, using the CONSTRAINED_INTERPOLATION keyword, a number of constraints are applied to the nodes at the free edges of the refined elements to keep them always upon the free edges of the coarse elements. The free edges of the elements involving the gaps are thus kept in contact during transient simulations.

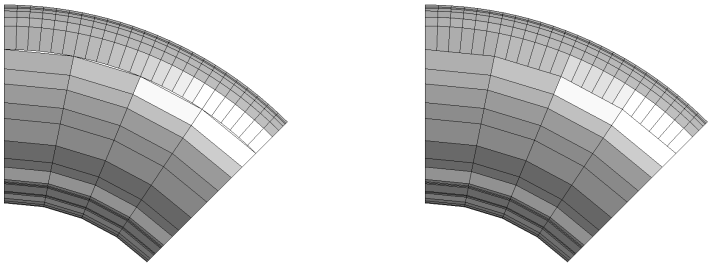

(a) Gaps due to mesh refinement (b) Mesh after obviating the gaps

Fig. 3: Gaps at the interface of the coarse and refined portions of the mesh and obviating them via modifying the nodal coordinates and applying constraints

The tire mesh in both models is then coupled with a rim, made of shell elements, via shared nodes so as to ensure tire-rim force transmission during simulations. The beads are thus not included in the models. The road is also considered as a rigid flat surface made of shell elements with 4-mm thickness.

2.2 Material Types and Properties

Both the tire models presented in this study use identical material types and properties. The rubber matrix in the carcass and belt plies is modeled using material type 1 (MAT_ELASTIC) from the LS-DYNA material library [21]. This material type requires the elastic properties of the rubber matrix forming the carcass and the belt plies, which are taken from the reported data [22] and listed in Table 2.

Table 2: Material properties of the carcass and belt rubber [22]

Property	Carcass rubber	Belt rubber
Density (ρ, $\mathrm{kg/m^3}$)	1190	1190
Young's modulus (E, MPa)	11.031612	13.789515
Poisson's ratio (ν)	0.49	0.49
Shear modulus (G, MPa)	3.701883	4.627354

The fiber-reinforced layers in the carcass and belt plies (Fig. 2) are modeled using material type 22 (MAT_COMPOSITE_DAMAGE), which simulates an orthotropic material with optional failure. This material type needs the orthotropic properties of the cord-rubber compounds in the carcass and belt plies, which are summarized in Table 3. These properties are computed based on the geometry and material data of the tire constituents including the twisted cords and the pure rubber, being reported in [13, 22], using the Halpin-Tsai equations following the methods proposed by Takeyama [18] and Walter [19]. Since these orthotropic properties are defined in the cord axes system (1,2,3), a cord angle is required to define the orientation of the cords with respect to the element axes system (x,y,z), as illustrated in Fig. 4.

Table 3: Material properties of the carcass and belt reinforcements

Property	Carcass reinforcement	Belt reinforcement
Density (ρ, $\mathrm{kg/m^3}$)	1810.5651	1910.2038
Young's Modulus (E_1, MPa)	7202.774505	14220.317525
Young's Modulus (E_2, MPa)	15.249372	20.190044
Poisson's Ratio ($\nu_{12} = \nu_{13}$)	0.4685	0.4645
Poisson's Ratio (ν_{23})	0.4217	0.4181
Shear Modulus ($G_{12} = G_{13}$)	4.645834	6.059683
Shear Modulus (G_{23}, MPa)	3.577292	4.605359

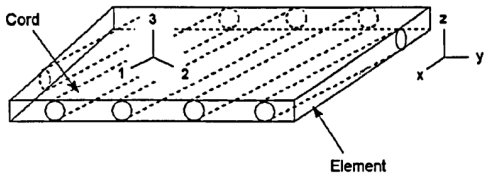

Fig. 4: Fiber-reinforced shell element [15]

The solid elements representing the bead fillers and the tread are modeled by the material type 27 (MAT_MOONEY_RIVLIN_RUBBER), which is considered to accurately describe the hyper-elastic behavior of the rubber in tire models [13, 15, 23]. Table 4 summarizes the material data for the bead fillers, the tread regions shown in Fig. 1, being taken from the reported data [23].

The shell elements representing the steel rim and the road are described using the material type 20 (MAT_RIGID) since these are substantially stiffer than the tire constituents. Based on the geometric and mass properties defined for different components, the weights of the tire and rim for both of the tire models were computed around 46 kg and 32 kg, respectively, which is in agreement with the 295/75R22.5 tire data [23].

Table 4: Material properties of the bead fillers and the tread

	Bead fillers		Tread base		Tread cap	
Regions	1	2 to 4	1	2 to 6	1	2 to 5
ρ, $\mathrm{kg/m^3}$	882	881	869	596	693	693
C_{10}, MPa	0.392	0.392	0.41	0.51	0.67	0.67
C_{01}, MPa	1.268	1.268	1.44	1.86	2.46	2.46
ν	0.499	0.499	0.499	0.499	0.499	0.499

2.3 Tire-Road Contact Model

The tire-road contact is modeled by defining the automatic surface to surface contact [24, 25] between the solid elements of the tire tread (as slave part) and the shell elements of the rigid road (as master part). The road friction is modeled using the Coulomb formulation, while the static and dynamic coefficients of friction are defined as 0.8 and 0.75 to represent dry asphalt [26].

2.4 Method of Analysis

2.4.1 Element Formulations

The carcass and belt fiber-reinforced shells in the Individual-Element (IE) model as well as the multi-layered shells in the Part-Composite (PC) model are modeled using the fully-integrated Belytschko-Tsay shell element formulation (type 16) [27]. In the Individual-Element (IE) model, for the rubber matrix in the carcass and belt plies, the one-point integration formulation would cause instabilities due to the aspect ratios being well above the desired unity values. Moreover, the fully-integrated element formulation could perform well only for lower speeds (< 50 km/h). Eventually, the thick-shell element formulation [25] could yield stable simulations for a rolling tire at high speeds up to 100 km/h. For the nearly-incompressible rubber materials in the tire tread and bead fillers (with ν near 0.5), the fully-integrated solid element formulation exhibited too stiff behavior and caused undesirable element locking resulting in numerical instabilities. The one-point-integration formulation, however, could yield stable and sufficiently accurate simulations with significant cost saving. The only disadvantage with this element formulation was the necessity to control the hourglass energy modes. One of the stiffness forms of the hourglass control (type 5) [25] was selected for the one-point integration elements representing rubber material, as it was reported that the default viscous form does not work well for rolling tires [15, 28]. The Belytschko-Tsay shell element formulation (type 2) [27] with one integration point was found enough for the rim and the road elements having rigid materials.

2.4.2 Types of Simulations

For both tire models, the explicit time integration method [25] is used for the dynamic analyses. The transient simulation is started by inflating the tire to a nominal pressure, i.e. 758 kPa (110 psi), via applying a uniformly distributed normal load to the shell elements of the inner layer of the tire. Following the tire stabilization after inflation, a vertical load is applied to the rim center in a ramp manner up to the desired load, e.g. 26.7 kN (6000 lb). Although a damping ratio of 0.05 is commonly adopted for truck tires [16, 23], a critical damping is applied to dampen the oscillations in the tire response quickly and thereby reduce the time required to converge to the steady-state deformation. The critical damping is computed based on the natural frequency corresponding to the first vertical free vibration mode of the tire, which can be obtained through conducting a modal analysis. As the tire approached its steady-state vertical deflection, the rolling phase of the tire is initiated, while the damping ratio was reduced to the typical value of 0.05. A free-rolling condition is simulated by applying a prescribed velocity, e.g. 50 km/h, to the road along the tire longitudinal axis, while the rim was only allowed to rotate about its axis. A side-slip situation can also be simulated by applying the road speed at a predefined angle, e.g. 6°, with respect to the tire heading direction. This approach permits the characterization of the cornering properties of the tire through measurements of the cornering force/moment at the ground contact. Eigenvalue analyses are performed to estimate the natural frequencies and mode-shapes of the tire models, while considering the effects by the inflation pressure, vertical load and contact boundary condition.

2.4.3 Mesh Size Selection

A grid study was conducted to meet the convergence of the simulation results versus mesh refinement. As shown in Fig. 5, different grids with varying number of circumferential divisions were considered, while the mesh of the outer circumferential regions remained fine (192 divisions) so as not to affect the tire-road contact algorithm during transient simulations. Fig. 6(a) illustrates the trend of convergence for the vertical tire deflection versus mesh refinement for both tire models. In these simulations, the tire was first inflated at a pressure of 758 kPa and was then vertically loaded at 26.7 kN. Moreover, Fig. 6(b) shows the convergence of the cornering force due to a 6° side-slip angle with the increase of mesh density for both tire models while being subjected to 758 KPa inflation and 26.7 kN load. Consequently, a grid with 96 sectors, being refined to 192 divisions for the outer regions, was selected as the minimum required mesh to be later employed in the load-deflection, cornering and modal analyses, as shown by Fig. 5(d).

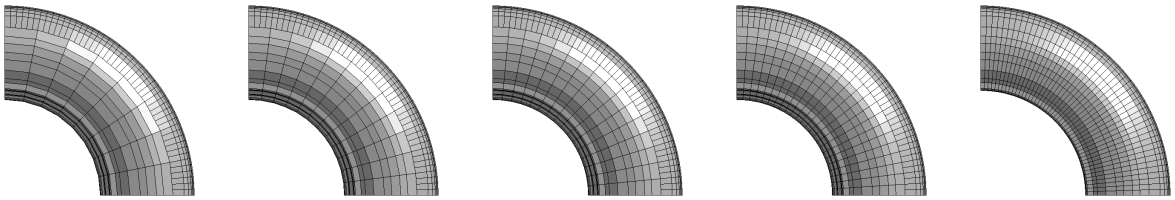

(a) $N_c = 32$ (b) $N_c = 48$ (c) $N_c = 64$ (d) $N_c = 96$ (e) $N_c = 192$

Fig. 5: Different grids with varying number of circumferential divisions used for grid study

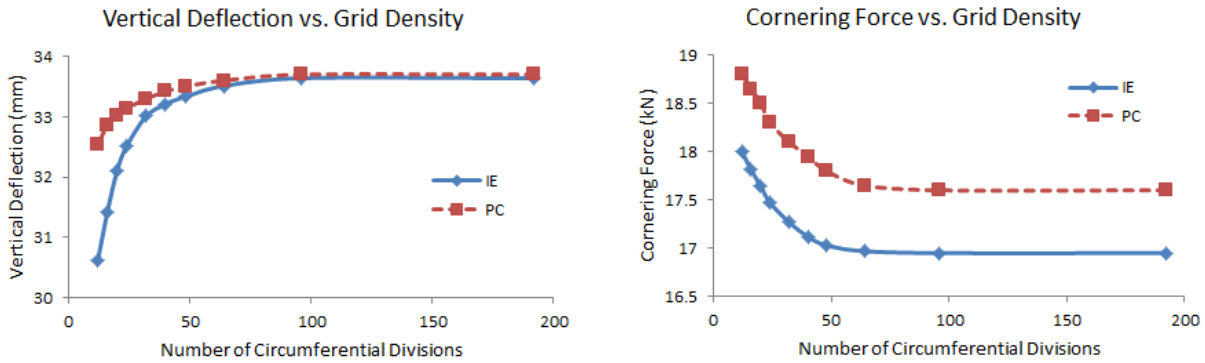

(a) Grid study on vertical deflection (b) Grid study on cornering force

Fig. 6: Grid study to determine the minimum number of circumferential divisions required for the convergence of the simulation results by the Individual-Element (IE) model and the Part-Composite (PC) model

3 Comparing Simulation Results

3.1 Comparing Load-Deflection Characteristics

The static vertical stiffness properties of both the tire models were evaluated through the load-deflection test, where the tire is first inflated at a specific pressure and is then deflected due to applying a vertical load. Fig. 7 compares the deformed shapes of the tire models under a 26.7 kN (6000 lb) vertical load, after being inflated at their nominal operating pressure, 758 kPa (110 psi).

Repeating the simulation for a range of vertical loads from 4.448 to 44.48 kN (1000 to 10000 lb), a load-deflection curve is obtained for characterizing the static vertical tire stiffness. Fig. 8 compares the load-deflection relations resulted from the two tire models at their nominal inflation pressure with the physical measurements provided by the Goodyear Tire and Rubber Company [29]. It not only verified the agreement between the two models in load-deflection characteristics, but also established the validity of their static vertical behavior.

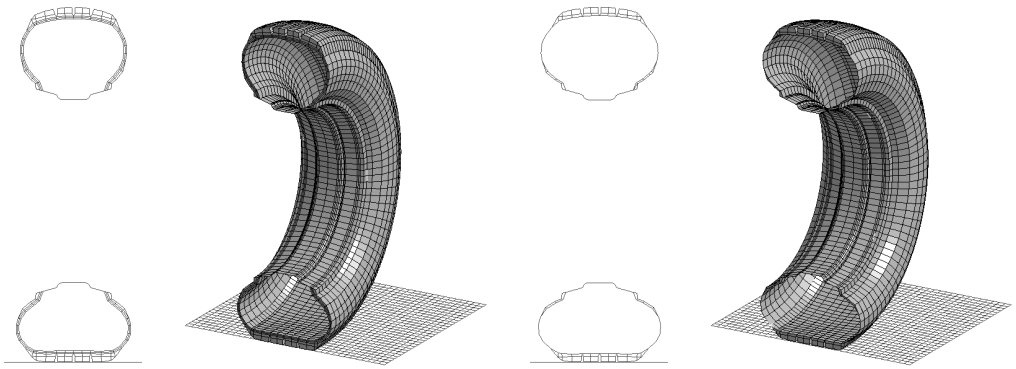

(a) Individual-Element (IE) model (b) Part-Composite (PC) model

Fig. 7: Deformed shape of the Individual-Element (IE) model and the Part-Composite (PC) model due to a 26.7 kN (6000 lb) vertical load at a 758 kPa (110 psi) inflation pressure

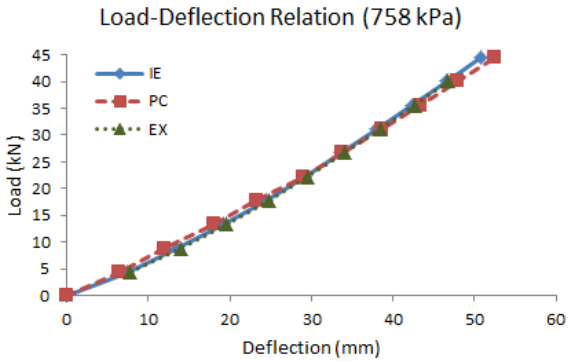

Fig. 8: Load-deflection relations at 758 kPa inflation pressure resulted from the Individual-Element (IE) model and the Part-Composite (PC) model and comparison with the experimental data (EX) reported in [29]

Moreover, Fig. 9 compares the load-deflection properties of the two tire models at inflation pressures other than nominal, i.e. 621 kPa (90 psi) and 896 kPa (130 psi). For a lower inflation pressure, as shown in Fig. 9(a), the perfect agreement of the models happens at higher loads; whereas for a higher inflation, as seen in Fig. 9(b), the models match well in the mid-range of vertical loads.

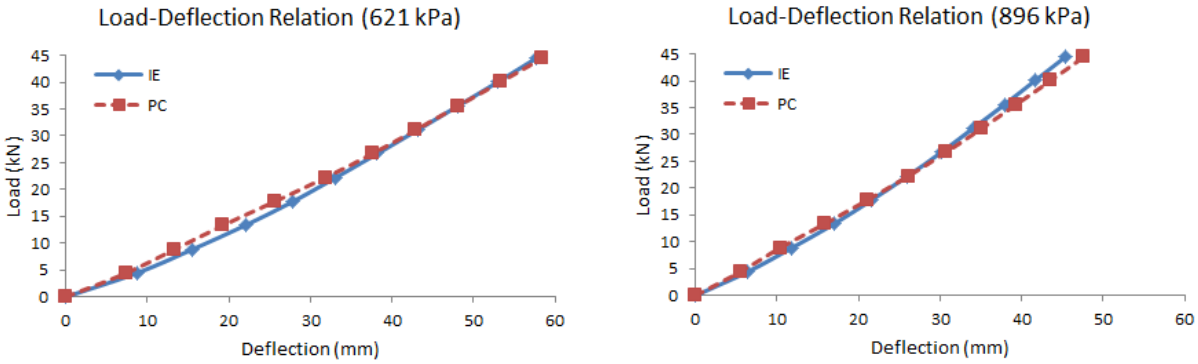

(a) At 621 kPa (90 psi) inflation pressure (b) At 896 kPa (130 psi) inflation pressure

Fig. 9: Comparing the load-deflection characteristics resulted from the Individual-Element (IE) model and the Part-Composite (PC) model at inflation pressures lower and higher than nominal

Using a 3.2 GHz Intel Xenon processor with 8 cores and 14 GB RAM, the computing time for a 0.2 sec load-deflection simulation was measured at 3:50 (235 minutes) for the Individual-Element (IE) model, which is 4.7 times longer than that of the Part-Composite (PC) model taking only 50 minutes. In these simulations, a mesh of 96 sectors was used, while the total number of elements for the IE and PC models were 24192 and 8832, respectively.

3.2 Comparing Cornering Characteristics

The cornering characteristics of both the tire models were evaluated through predicting the cornering forces/moments generated due to a wide range of constant side-slip angles up to 12°. The side-slip situations were produced through applying a 5 km/h speed to the road at predefined angles with respect to the tire heading direction, while the tire was allowed to roll freely after it was deflected via applying a prescribed 33.64 mm z-motion to the rim (corresponding to a 26.7 kN vertical load). In these simulations, the static and dynamic coefficients of friction were assumed as 0.8 and 0.75, respectively, to represent dry asphalt [26]. The cornering simulations were performed at the nominal inflation pressure (758 kPa).

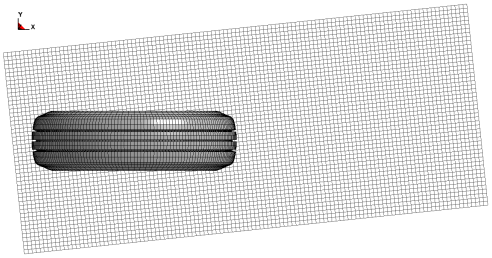

Fig. 10: Free-rolling at constant side-slip angle (6°)

Fig. 11 compares the cornering forces as well as the aligning moments predicted by the two models with the experimental data provided by the University of Michigan Transportation Research Institute [29]. The two models exhibited good agreements with each other in both the cornering force and the aligning moment results. However, in comparison with the experimental data, the correspondence of the results predicted by the models in the cornering force was much better than that in the aligning moment. In the mid-range of side-slip angles (around 6°), both the tire models predicted the cornering forces in perfect agreement with the experimental data, while slightly overestimating them at lower side-slip angles and underestimating at higher ones. At higher side-slip angles, the cornering forces predicted by the models converged to a certain level, while the experimental results still had tendency to grow up. The aligning moments predicted by the models matched with the experimental data only qualitatively in trends except for the lower side-slip angles ($< 4^\circ$) at which showed reasonable quantitative agreements as well.

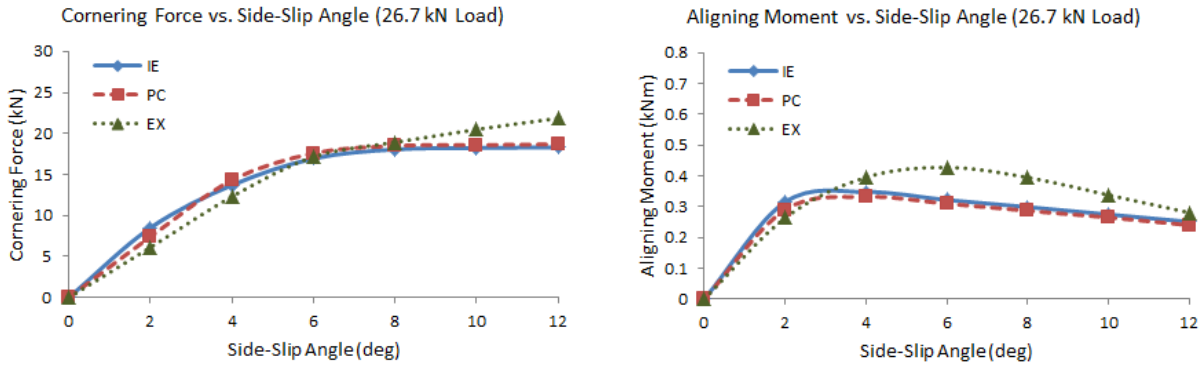

(c) Cornering force (d) Aligning moment

Fig. 11: Cornering characteristics at 5 km/h speed and 26.7 kN load resulted by the Individual-Element (IE) model and the Part-Composite (PC) model and comparisons with the experimental data (EX) [29]

Using a 3.2 GHz Intel Xenon processor with 8 cores and 14 GB RAM, the computing time for a 1.0 sec cornering simulation was measured at 16:45 (1005 minutes) for the Individual-Element (IE) model, which is 5.9 times longer than that of the Part-Composite (PC) model taking only 2:50 (170 minutes). In these simulations, a mesh of 96 sectors was used, while the total number of elements for the IE and PC models were 24192 and 8832, respectively.

3.3 Comparing Modal Characteristics

Eigenvalue analyses were performed to compare the modal behavior of the two tire models. The intermittent eigenvalue extraction option [25] was employed so as to include the effects of the tire inflation pressure, vertical load and contact boundary condition in the modal analyses. This option was activated via choosing the parameter IMFLAG as 6 in the CONTROL_IMPLICIT_GENERAL keyword. Using this option, an eigenvalue analysis can be performed at a certain time during a transient simulation in order to include the effects of all loadings and boundary conditions in the analysis. In the load-deflection test simulations, while the tire models were steadied after applying the inflation pressure and the vertical load, the intermittent eigenvalue extractions were executed. Table 5 compares the natural frequencies resulted from the modal analyses performed on the two tire models, while they are inflated at 758 kPa and vertically loaded at 26.7 kN. Figures 12 and 13 illustrate the mode shapes corresponding to the in-plane and out-of-plane vibration modes listed in Table 5. The natural frequencies resulted from the two models showed perfect agreement for the in-plane vibration modes, while there were some discrepancies (< 7%) between the results for the out-of-plane modes.

Table 5: Natural frequencies (Hz) resulted from the modal analyses performed on the Individual-Element (IE) model and the Part-Composite (PC) model

In-Plane Modes				Out-of-Plane Modes			
Mode	IE	PC	Error	Mode	IE	PC	Error
(a) Hop	17.85	17.76	-0.5%	(a) Translate Y	45.21	42.58	-5.8%
(b) Rotate Y	49.47	49.79	0.6%	(b) Rotate Z	50.84	49.85	-2.0%
(c) Oval	76.97	77.36	0.5%	(c) Oval	78.03	82.07	5.2%
(d) Triangle	102.25	101.71	-0.5%	(d) Triangle	112.20	119.52	6.5%
(e) Quad	110.25	109.57	-0.6%	(e) Quad	129.12	138.12	6.9%

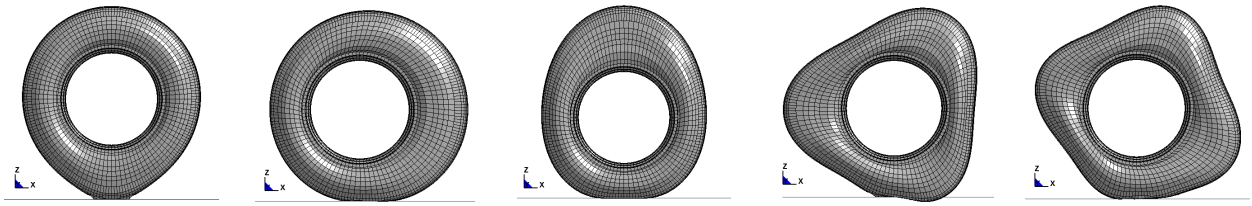

(a) Hop (b) Rotate Y (c) Oval (d) Triangle (e) Quad

Fig. 12: Vibration mode shapes related to in-plane modes

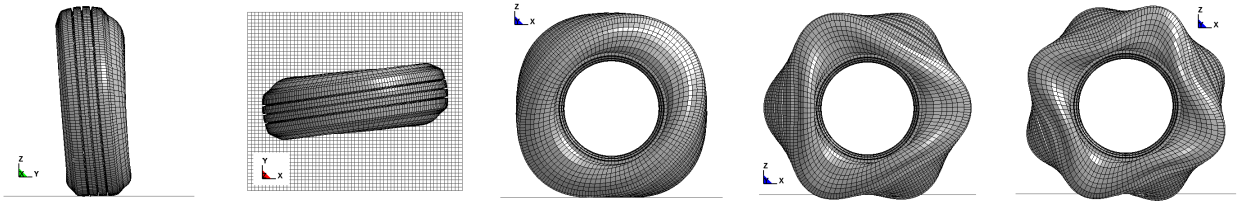

(a) Translate Y (b) Rotate Z (c) Oval (d) Triangle (e) Quad

Fig. 13: Vibration mode shapes related to out-of-plane modes

4 Summary

In this study, the Part-Composite approach in LS-DYNA was verified to be applicable in modeling the multi-layered composite structure of a rolling truck tire. In order to evaluate the ability of the Part-Composite alternative in managing a stack of different layers with a single shell element, it was compared to a much more detailed method which employed individual elements for modeling different layers in the tire structure. Both the models used the same configuration of layers with identical materials, thicknesses and fiber orientations. The simulation results obtained by the two tire models were compared with each other as well as with the reported experimental data in terms of the load-deflection, cornering force/moment and vibration characteristics. The load-deflection properties of the two tire models were verified to be in perfect agreement with each other as well as with the experimental data, which established the validity of the tire models in static vertical behavior. The cornering force and the aligning moment characteristics of the two models were shown to be in good agreement with each other. However, only the cornering forces matched with the experimental data. The aligning moments agreed well with the measurements qualitatively in trends and the quantitative correspondence only happened at the side-slip angles below 4°. Using the intermittent eigenvalue analysis, the modal properties of the tire models were determined, while the effects of the inflation pressure and vertical load were also included. The natural frequencies resulted from the two models showed perfect agreement for the in-plane vibration modes, while there were some discrepancies (< 7%) between the results for the out-of-plane modes. Using the Part-Composite (PC) model, the total number of elements was reduced by 63%, which remarkably improved the computational efficiency so that the required CPU time was reduced by 79% in a load-deflection test and by 83% in a cornering simulation.

References

[1] K. M. Captain, A. B. Boghani, and D. N. Wormley, “Analytical tire models for dynamic vehicle simulation,” *Vehicle System Dynamics*, vol. 8, no. 1, pp. 1–32, 1979.

[2] M. Loo, “A model analysis of tire behavior under vertical loading and straight-line free rolling,” *Tire Science and Technology*, vol. 13, no. 2, pp. 67–90, 1985.

[3] J. Kisilowski and Z. Lozia, “Modelling and simulating the braking process of automotive vehicle on uneven surface,” *Vehicle System Dynamics*, vol. 15, no. S1, pp. 250–263, 1986.

[4] K. Guo and Q. Liu, “A model of tire enveloping properties and its application on modeling of automobile vibration systems,” *SAE Technical Paper, 980253*, 1998.

[5] P. W. A. Zegelaar and H. B. Pacejka, “The in-plane dynamics of tyres on uneven roads,” *Vehicle System Dynamics*, vol. 25, no. S1, pp. 65–79, 1996.

[6] J. P. Maurice, *Short wavelength and dynamic tyre behavior under lateral and combined slip conditions*. Ph.d. dissertation, Delft University of Technology, 2000.

[7] H. B. Pacejka and E. Bakker, “The magic formula tire model,” *Vehicle System Dynamics*, vol. 21, no. 1, pp. 1–18, 1992.

[8] S. Bruni, F. Cheli, and F. Resta, “On the identification in time domain of the parameters of a tyre model for the study of in-plane dynamics,” *Vehicle System Dynamics*, vol. 27, no. S1, pp. 136–150, 1997.

[9] J. J. M. Van Oosten and E. Bakker, “Determination of magic tyre model parameters,” *Vehicle System Dynamics*, vol. 21, no. S1, pp. 19–29, 1992.

[10] M. Shiraishi, H. Yoshinaga, N. Iwasaka, and K. Hayashi, “Making FEM tire model and applying it for durability simulations,” in *6th International LS-DYNA Users Conference*, (Detroit), 2000.

[11] T. Fukushima and H. Shimonishi, “Vehicle turn simulation using FE tire model,” in *LS-DYNA Anwenderforum*, (Bamberg), 2004.

[12] M. Shiraishi, N. Iwasaka, T. Saruwatari, and K. Hayashi, “Developing a FE-Tire model library for durability and crash simulations,” in *7th International LS-DYNA Users Conference*, 2001.

[13] X. Zhang, S. Rakheja, and R. Ganesan, "Nonlinear finite element modeling and incremental analysis of a truck tire," *Heavy Vehicle Systems*, vol. 9, no. 3, pp. 253–279, 2002.

[14] X. Yan, "Nonlinear three-dimensional finite element analysis of steady rolling radial tires," *Journal of reinforced plastics and composites*, vol. 22, no. 8, pp. 733–750, 2003.

[15] W. Hall, J. T. Mottram, and R. P. Jones, "Tire modeling methodology with the explicit finite element code LS-DYNA," *Tire Science and Technology*, vol. 32, no. 4, pp. 236–261, 2004.

[16] S. Chae, M. El-Gindy, M. Trivedi, I. Johansson, and F. Öijer, "Dynamic response predictions of a truck tire using detailed finite element and rigid ring models," in *ASME 2004 International Mechanical Engineering Congress and Exposition*, pp. 861–871, American Society of Mechanical Engineers, 2004.

[17] R. Ali, R. Dhillon, M. El-Gindy, F. Öijer, I. Johanson, and M. Trivedi, "Prediction of rolling resistance and steering characteristics using finite element analysis truck tyre model," *International Journal of Vehicle Systems Modelling and Testing*, vol. 8, no. 2, pp. 179–201, 2013.

[18] T. Takeyama, J. Matsui, and M. Hijiri, *Mechanics of Pneumatic Tires*, ch. Tire Cord and Cord to Rubber Bonding, Chapter 2. Washington DC: U.S. Department of Transportation, National Highway Traffic Safety Administration (NHTSA), 1981.

[19] J. D. Walter, *Mechanics of Pneumatic Tires*, ch. Cord Reinforced Rubber, Chapter 3. Washington DC: U.S. Department of Transportation, National Highway Traffic Safety Administration (NHTSA), 1981.

[20] J. D. Reid, D. A. Boesch, and R. W. Bielenberg, "Detailed tire modeling for crash applications," *International Journal of Crashworthiness*, vol. 12, no. 5, pp. 521–529, 2007.

[21] "Ls-dyna keyword user's manual, volume 2: Material models, version 971." Livermore Software Technology Corporation, California, March 2012.

[22] S. K. Clark, *Mechanics of Pneumatic Tires*. Washington DC: U.S. Department of Transportation, National Highway Traffic Safety Administration (NHTSA), 1981.

[23] S. Chae, J. Allen II, F. Öijer, M. El-Gindy, M. Trivedi, and I. Johansson, "Dynamic response predictions of quarter-vehicle models using FEA and rigid ring truck tire models," in *ASME International Mechanical Engineering Congress and Exposition*, (Illinois), American Society of Mechanical Engineers, 5–10 November 2006 2006.

[24] J. O. Hallquist, "Ls-dyna theory manual." Livermore Software Technology Corporation, California, 2006.

[25] "Ls-dyna keyword user's manual, volume 1, version 971." Livermore Software Technology Corporation, California, September 2012.

[26] J. Y. Wong, *Theory of Ground Vehicles*. New York: John Wiley & Sons, 4th ed. ed., 2001.

[27] T. Belytschko, J. Lin, and C. S. Tsay, "Explicit algorithms for the nonlinear dynamics of shells," *Computer Methods in Applied Mechanics and Engineering*, vol. 42, pp. 225–251, 1984.

[28] W. Hall, J. T. Mottram, and R. P. Jones, "Finite element simulation of a rolling automobile tyre to understand its transient macroscopic behavior," in *Proceedings of the Institution of Mechanical Engineers, Part D: Journal of Automobile Engineering*, vol. 218, pp. 1393–1408, SAGE Publications, December 2004.

[29] S. Chae, *Nonlinear Finite Element Modeling and Analysis of a Truck Tire*. Ph.d. dissertation, Pennsylvania State University, USA, 2006.

